Updating Historical Maps of Malaria Transmission Intensity in East Africa Using Remote Sensing

J.A. Omumbo, S.I. Hay, S.J. Goetz, R.W. Snow, and D.J. Rogers

Abstract

Remotely sensed imagery has been used to update and improve the spatial resolution of malaria transmission intensity maps in Tanzania, Uganda, and Kenya. Discriminant analysis achieved statistically robust agreements between historical maps of the intensity of malaria transmission and predictions based on multitemporal meteorological satellite sensor data processed using temporal Fourier analysis. The study identified land surface temperature as the best predictor of transmission intensity. Rainfall and moisture availability as inferred by cold cloud duration (CCD) and the normalized difference vegetation index (NDVI), respectively, were identified as secondary predictors of transmission intensity. Information on altitude derived from a digital elevation model significantly improved the predictions. "Malaria-free" areas were predicted with an accuracy of 96 percent while areas where transmission occurs only near water, moderate malaria areas, and intense malaria transmission areas were predicted with accuracies of 90 percent, 72 percent, and 87 percent, respectively. The importance of such maps for rationalizing malaria control is discussed, as is the potential contribution of the next generation of satellite sensors to these mapping efforts.

Introduction

Human malaria is caused by the parasites *Plasmodium falciparum, P. vivax, P. ovale*, and *P. malariae*. The Plasmodium life cycle involves an asexual stage in human hosts and a sexual stage in mosquitoes of the genus Anopheles. *Anopheles gambiae* sensu stricto and *An. funestus* are the most widely distributed and important malaria vectors in sub-Saharan Africa (SSA). Ninety percent of the global burden of malaria, predominantly due to *P. falciparum*, is borne by the population of SSA (WHO, 1999), resulting in approximately 1 million deaths due to *P. falciparum* each year (Snow *et al.*, 1999). The clinical spectrum of *P. falciparum* infection ranges in severity from mild, often self-limiting, fever, chills, and joint pains to a life-threatening illness.

Malaria transmission is often quantified through mathematical models. The basic reproductive number of a disease (R_0) is derived from a generic infectious disease model and is defined as the average number of successful offspring that a parasite is intrinsically capable of producing in a completely susceptible population (Macdonald, 1957). The vectorial capacity (VC), derived from R_0, reflects the mean number of probable inoculations transmitted from one case of malaria per unit time (Garrett-Jones, 1964) and it is expressed as

$$\mathrm{VC} = \frac{ma^2p^n}{-\log_e p} \tag{1}$$

where m is the relative density of female anophelines, a is the probability that the mosquito will take a human blood meal during a particular day, and p^n is the proportion of vectors surviving the parasite's incubation period (i.e., p is the daily probability of vector survival and n is the duration of parasite sexual development within the mosquito or sporogony). All of these factors, with the possible exception of a, are affected by climate and hence environmental proxy information derived from satellite sensors (Hay *et al.*, 1996; Hay *et al.*, 1999) can be of use in predicting malaria transmission intensities (Hay *et al.*, 1997; Rogers *et al.*, 2002).

Optimum temperatures for *P. falciparum* (sporogony) are between 25 and 30 °C. Below 16 °C and above 35 °C sporogony ceases (Detinova, 1962), and thermal death of mosquitoes occurs at 40 to 42 °C (Dutta *et al.*, 1978). Breeding site availability is associated with rainfall and increased mosquito survivorship with increasing humidity (Gill, 1920; Dutta *et al.*, 1978). Non-climatic factors, including proximity to permanent water bodies, urbanization, population distribution, agricultural practices, and other human factors, further modify transmission (Gilles, 1993). The spatial heterogeneity of these factors contributes substantially to variations in transmission intensity. For example, one marker of malaria transmission intensity, the annual entomological inoculation rate (EIR) defined as the average number of infective mosquito bites received per

J.A. Omumbo and S.I. Hay are with the Trypanosomiasis and Land-Use in Africa (TALA) Research Group, Department of Zoology, University of Oxford, South Parks Road, Oxford OX1 3PS, United Kingdom and with the Kenya Medical Research Institute/Wellcome Trust collaborative programme, P.O. Box 43640, Nairobi, Kenya (judith.omumbo@zoology.oxford.ac.uk).

S.J. Goetz is with the Department of Geography, University of Maryland, College Park, Maryland, MD 20742-8225.

R.W. Snow is with the Kenya Medical Research Institute/Wellcome Trust collaborative programme, P.O. Box 43640, Nairobi, Kenya and with the Centre for Tropical Medicine, University of Oxford, John Radcliffe Hospital, Headington, Oxford, OX3 9DU, United Kingdom.

D.J. Rogers is with the Trypanosomiasis and Land-Use in Africa (TALA) Research Group, Department of Zoology, University of Oxford, South Parks Road, Oxford OX1 3PS, United Kingdom.

Photogrammetric Engineering & Remote Sensing
Vol. 68, No. 2, February 2002, pp. 161–166.

0099-1112/02/6800–161$3.00/0

person in a year) ranges from 0 to ~1000 across sub-Saharan Africa (Hay *et al.*, 2000b). This heterogeneity is best captured by maps which themselves should form an important tool for rationalizing malaria control (Snow *et al.*, 1996).

Several authors have attempted to describe the global distribution of malaria using expert opinion and climate data. Early maps were based on the position of summer isotherms (Boyd, 1930; Lysenko *et al.*, 1969); the known latitudinal extent of the disease (Gill, 1920); combinations of temperature, elevation, and rainfall (Dutta *et al.*, 1978); and interpolation of limited malariometric data (Clyde, 1967; Onori, 1967). In recent years there has been a renaissance in mapping malaria in Africa (Snow *et al.*, 1996; MARA/ARMA collaboration, 1998; Hay *et al.*, 2000a; Rogers *et al.*, 2002). This has been facilitated by advancements in geographic information systems (GIS) and increased availability of public domain, remotely sensed (RS) satellite data. RS surrogates of climate have been used to develop high spatial resolution maps of transmission intensity and epidemic potential (Lindsay *et al.*, 1996; Snow *et al.*, 1998; Craig *et al.*, 1999; Thomson *et al.*, 1999; Kleinschmidt *et al.*, 2000). In this paper we discuss the utility of remote sensing for re-visiting historical efforts to describe malaria distribution in East Africa at high spatial resolution.

Materials and Methods

Historical Malaria Distribution Maps

At the time of independence, concerted efforts were made to provide atlases for use in administration and development planning in Tanzania, Uganda, and Kenya (Government of Tanganyika, 1956; Government of Uganda, 1962; Government of Kenya, 1970). The atlases included maps of synoptic rainfall and temperature, health facilities, agriculture, natural resources, and malaria. The rules used to categorize malaria transmission differed slightly between the three countries, but all were derived from expert opinion on climate and local malariology.

Uganda's map (Government of Uganda, 1962) describes four malaria epidemiological zones as follows: (1) *normally malaria free*: highland areas above 1500 meters where transmission is limited by low temperatures, (2) *malarious near water*: arid sparsely populated areas where transmission occurs only around permanent water bodies, (3) *moderately malarious*: areas experiencing warm moist climate with evenly distributed moderate rainfall where malaria transmission is seasonal, and (4) *intensely malarious*: areas below 1500 meters where transmission occurs year round, increasing after periods of heavy rainfall. In both Kenya (Government of Kenya, 1970) and Tanzania (Government of Tanganyika, 1956), five zones are defined according to the duration of the transmission season as follows: (i) *Transmission for less than three months of a year*; (ii) *transmission for three to six months*; (iii) *transmission for more than six months of a year*; (iv) *malarious near water*; and (v) *malaria free*: highland areas, although a precise altitude limit is not indicated in the definition.

To provide uniform categories of malaria transmission for analysis, slight reclassifications were necessary so that maps of malaria transmission intensity in Kenya and Tanzania could be directly compared with those for Uganda. This was justified by recent work suggesting that the "intensity" of transmission is strongly correlated with the length of the malaria transmission season (Tanser, 2000). Areas experiencing transmission for more than 6 months were reclassed as "intensely malarious," areas with transmission for less than 3 months and for 3 to 6 months were combined and reclassed as "moderately malarious," and areas defined as malaria-free and malarious near water remained unchanged. The historical maps were digitized using the GIS MapInfo (MapInfo Corporation, 1985–2000) and the vector map was rasterized using IDRISI version 2.1 (Clarke University, 1997).

The Pathfinder Advanced Very High Resolution Radiometer Land (PAL) Data

This study uses data derived from the National Oceanic and Atmospheric Administration (NOAA) Advanced Very High Resolution Radiometer (AVHRR) sensor on board the NOAA series of polar-orbiting satellites. Public domain 8- by 8-km spatial resolution satellite data were obtained through the Pathfinder AVHRR Land (PAL) program (James *et al.*, 1994; URL: http://daac.gsfc.nasa.gov/data/dataset/AVHRR/index.html). These data were processed using standard quality control and cloud reducing procedures outlined in Hay *et al.* (1999).

Normalized Difference Vegetation Index

Of the many spectral vegetation indices available, the Normalized Difference Vegetation Index (NDVI) (Tucker, 1979) has found most application in epidemiological studies (Hay *et al.*, 1998; Patz *et al.*, 1998; Snow *et al.*, 1998; Kleinschmidt *et al.*, 2000). As a robust indicator of photosynthetic activity (Tucker *et al.*, 1986; Myneni *et al.*, 1995), it is thought to provide information on the response of a landscape to precipitation (Nicholson *et al.*, 1990) and is hence of use in malaria studies. The NDVI is derived from AVHRR channels 1 (visible) and 2 (near-infrared) as follows:

$$\text{NDVI} = \frac{\text{Ch2} - \text{Ch1}}{\text{Ch2} + \text{Ch1}}. \tag{2}$$

Mid-Infrared (MIR) Reflectance

AVHRR channel 3 (mid-infrared) has been shown to be sensitive to both reflected and emitted radiation, although the interpretation of this signal is less well understood than the other channels (Boyd *et al.*, 1998). MIR suffers less from atmospheric attenuation than do channels 4 and 5 of the AVHRR (Cracknell, 1997) and has found limited use for vegetation mapping.

Land Surface and Air Temperature Indices

The land surface brightness temperature (LST) was calculated using the "split-window" equation of Price (1984) as follows:

$$\text{LST} = T_{\text{Ch4}} + 3.33(T_{\text{Ch4}} - T_{\text{Ch5}}). \tag{3}$$

This has been found to be a relatively accurate proxy of ground-based meteorological measurements of air temperature with a root-mean-square error of ±4 °C over continental Africa (Hay *et al.*, 2000a). A further air temperature variable (T_{air}) was estimated using a contextual combination of vegetation indices and LST estimates reviewed by Goetz *et al.* (2000).

Altitude

A 1- by 1-km spatial resolution digital elevation model (DEM) for Africa was obtained from the United States Geological Survey (USGS) (Gesch *et al.*, 2000; URL: http://edcdaac.usgs.gov/gtopo30/README.html). Elevation is recorded in meters above sea level with a root-mean-square error reported at ±100 meters.

Rainfall

A proxy for rainfall can be derived from the European Organisation for the Exploitation of Meteorological Satellites (EUMESAT) Meteosat series. The exact threshold temperature associated with rain-bearing clouds and the quantity of rain they deposit varies temporally and spatially so that it must be established empirically. This has been done for Africa by the Tropical Applications of Meteorology using Satellite and other data (TAMSAT) programme of the Department of Meteorology, University of Reading (URL: http://www.met.reading.ac.uk/famsat). The northern and southern extent of the calibration

exercise represents the most northern and southern limits of the Inter Tropical Convergence Zone (ITCZ) where convective atmospheric processes dominate (Dugdale *et al.*, 1995). There are set thresholds of −50 °C in the summer and −60 °C in the winter, used for areas north of the ITCZ, and −40 °C throughout the year for regions south. These results were used by the FAO-ARTEMIS project to generate monthly cold cloud duration (CCD) images, where each pixel represents the number of hours during which cold cloud-top temperatures were below these thresholds during a 10-day compositing period. The CCD has been found to have a root-mean-square error of ±38 mm when compared with meteorological station recordings of rainfall across continental Africa (Hay *et al.*, 1999).

Data Preparation and Analysis

The AVHRR data are supplied in the equal-area Goode's interrupted homolosine projection. All images were reprojected to a Latlong coordinate system. The area covering East Africa (29°E to 42°E and 11.8°S to 5.5°N) was subset for further analysis. Temporal Fourier analysis (TFA) (Rogers *et al.*, 1996; Rogers, 2000) was applied to the five-predictor variables, NDVI, MIR, LST, T_{air}, and CCD. TFA summarizes the time series data using a series of sine and cosine functions. The periodic part of the time series is isolated and described by its frequency (annual, biannual, or triannual), amplitude (amp), and phase (phs). Ten Fourier images (mean, maximum, minimum, and variance; amplitudes of annual, biannual, and triannual cycles; and phases of annual, biannual, and triannual cycles) were produced for each predictor variable.

A randomly sampled "training data" set was selected from the historical distribution maps. Image pixels along the boundaries of malaria categories were excluded from the sampling frame because such areas have a high probability of misclassification of malaria intensity. Areas covered by large permanent water bodies were also excluded. Nine-hundred seventy-five training data pixels were selected; three-hundred for each of the categories "malaria near water," "moderate malaria," and "intense malaria." The "malaria-free" category covered a much smaller area, so only 75 training data pixels were selected. Corresponding values of the predictor variables were extracted for each of the 975 training data pixels.

The *kappa* statistic (Cohen, 1960) was selected as a measure of agreement. Values of *kappa* less than 0.4 indicate poor agreement, values between 0.4 and 0.75 suggest good agreement, and values above 0.75, excellent agreement (Landis *et al.*, 1977). Using discriminant analysis (DA), predictor variables were selected in a forward step-wise fashion by iteratively including the variable that causes the maximum increase in the *kappa* statistic (Cohen, 1960) compared with the other variables in each round of analysis until ten variables were selected. As the environmental characteristics within the different malaria regions are dissimilar, DA was carried out with the assumption of different covariance matrices between the malaria groups. It was also assumed that the *a priori* probabilities of group membership were equal. Based on the discriminant function, each pixel was assigned a malaria category. A map of the *a posteriori* probabilities was then plotted for East Africa and compared with the historical map.

Results

Pixels contaminated with water and those with predictor variable values greater than 6 standard deviations from means were excluded ($n = 4$). Nine-hundred seventy-one pixels were used in the analysis. Temperature variables were strongly correlated (Pearson correlation coefficients of 0.99 for mean Price LST and mean MIR reflectance; 0.81 for mean LST and mean T_{air}; and 0.77 for mean MIR reflectance and mean T_{air} (Table 1)). A strong negative correlation (−0.67) was found between altitude and T_{air}. Moisture availability surrogates were not as strongly correlated, the highest correlations being CCD amp1 and NDVI amp1 (0.71) and NDVI mean and CCD mean (0.64). Non-significant correlations were noted between malaria intensity class and the NDVI and CDD variables (coefficients less than 0.5).

TABLE 1. CORRELATION COEFFICIENTS OF INDEPENDENT VARIABLES

	Altitude	Mean MIR reflectance	Mean Price LST	Mean NDVI	NDVI amp1
Mean MIR reflectance	−0.50				
Mean Price LST	−0.59	0.99			
Mean T_{air}	−0.67	0.77	0.81		
Mean CCD				0.64	
CCD amp1					0.71

Plots of the predictor variables by malaria intensity class showed considerable overlap in environmental conditions between the four malaria categories except with regard to temperature (mean Price LST) and altitude. Average and ranges of mean LST distinguish well between the "malaria-free" and "malaria near water" categories compared with other malaria classes (Figure 1). The altitude differences between these categories are also shown in Figure 1.

In the discriminant analysis overall agreement between training data (observed) and predicted pixels was 89.9 percent (Cohen's *kappa* = 0.775; Klecka's *tau* = 0.773), with greatest agreement in the categories "malaria-free" and "malaria near water" (Table 2). The model over predicted "malaria-free" areas (false positive rate = 26.3 percent) and under predicted moderate malaria (false negative rate = 27.7 percent (Table 3)).

Table 4 lists the top ten RS variables selected by the DA, and minimum, maximum, and mean values for these. Six of these are temperature variables (LST, DEM, T_{air}, and MIR reflectance) while CCD variables appear three times. The DA was repeated omitting some of the strongly correlated variables (T_{air} and/or mean MIR reflectance). In each case the mean Price LST was most discriminating. Considerably higher misclassification rates were obtained when T_{air} or MIR reflectance variables were omitted from the discriminant analysis. The DA was also done using only the first five discriminating variables; however, the resulting *a posteriori* predictions were poorer (*kappa* = 0.706). Including all ten variables produced the best fit, with an overall kappa of 0.775.

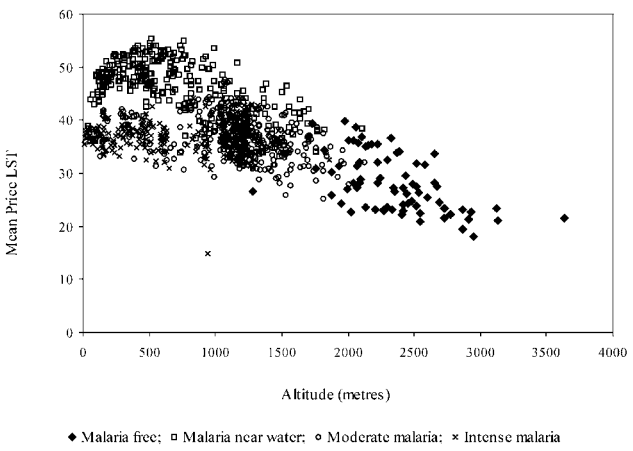

Figure 1. Relationship between land surface temperature (Price, 1984), altitude, and historical classifications of malaria transmission intensity.

TABLE 2. CLASSIFICATION MATRIX FOR TRAINING DATA AND PREDICTED PIXELS

		Predicted				
	Malaria intensity	Malaria free	Malaria near water	Moderate	Intense	Total
Observed	Malaria free	70	0	2	1	73
	Malaria near water	9	270	12	9	300
	Moderate malaria	15	15	217	53	300
	Intense malaria	1	2	37	258	298
	Total	95	287	268	321	971

Cohen's *kappa*: 0.775 (Cohen, 1960), Klecka's *tau*: 0.773. Also see Table 3.

Figure 2a shows the rasterized historical transmission map with major water bodies overlaid. (The national boundaries used are as they were at the time the historical maps were printed, and changes have since occurred along Kenya's northwestern border with Sudan.) The Tana River in eastern Kenya drains into the Indian Ocean through an arid, low altitude (less than 400 m above sea level) region. According to the historical map, intense malaria transmission occurs within a narrow band (less than 5 km) along the riverbank. Areas of differing malaria transmission intensity are color coded as follows: malaria free (white), malaria near water (light grey), moderate malaria (dark grey), and intense malaria (black). The "malaria-free" areas on the map have an average altitude of 2335 meters (range 1282 to 3634 meters) while the "malaria near water" areas average 680 meters (range 14 to 1800 meters).

Discussion

The DA was carried out using different numbers and combinations of predictor variables. The prediction resulting in the highest kappa statistic (Figure 2b) is compared with the historical map (Figure 2a). Predictions were best at the extremes of transmission and in areas that experience very characteristic environmental or climatic conditions. For example, arid areas (transmission occurring only in proximity to per-manent water bodies) experience year-round high temperatures, and the thermal indices therefore identify these areas well. Similarly, "malaria-free" areas are typically at high altitude and are characterized by much lower year-round temperatures (Figure 1). In moderate and intense transmission areas, such distinction of environmental characteristics is not as pronounced. Although the main areas of malaria transmission intensity are well predicted, the boundaries within moderate transmission areas are much less distinct, such as the Indian Ocean coastline on Kenya's southeastern border, parts of western Uganda, and large areas of central Tanzania. Incorporation of an environmental zone classification variable into the DA as an additional predictor variable may allow more of the environmental differences between moderate and intense transmission classes to be isolated (Brooker *et al.*, 2002).

It is important to note that the historical transmission maps were based largely on expert opinion and were intended to provide only a broad representation of available information on the distribution and intensity of malaria. Criteria used for classification varied between the three countries. Tanzania's map was based predominantly on the expert opinion of a malaria epidemiologist and, on this basis, areas along rivers are classed as intense transmission areas (Figure 2c) as was done with the Tana River in Kenya. Most misclassified pixels are found in Tanzania mainly along rivers and on the margins of transmission categories (Figure 2c), suggesting that additional factors, not identified by climatic predictors, determine transmission intensity. The masking of a row of 8- by 8-km pixels along the boundaries of the transmission categories ex-cluded the Tana River banks from the sampling frame, resulting in the omission of the river on the predictive map. It is possible that several other areas on the historical map where transmission occurs alongside rivers (particularly in Tanzania) should have been left out for similar reasons. Uganda's map is influenced largely by expert knowledge of altitude and rainfall distribution and their relationship to malaria transmission. Regions of similar climate are grouped together; as for example, areas experiencing "Lake Victoria weather" are described. Malaria intensity regions were classified on the basis of such similarity of climatic conditions. Kenya's map was designed to identify persons "at risk" according to ethnic groupings, and the malaria map has been influenced by the pattern of these settlements.

There are several advantages of the approach used here over previous attempts at modeling. First, RS data provide a continuous surface, thus avoiding the use of interpolated climate data with its inherent interpretation biases; also, high temporal resolution climate data have been used. Fourier processed imagery, by summarizing climatic data according to its natural biological cycles, better relates to the biological processes involved in malaria transmission. Rainfall patterns in East Africa show a bimodal distribution (two rainy seasons in a year) in most areas, and this may be related to the selection of the timing of CCD biannual cycles and NDVI by the discriminant analysis. Although temperatures in arid areas tend to be high

TABLE 3. AGREEMENT BETWEEN HISTORICAL AND PREDICTED MAP OF MALARIA TRANSMISSION INTENSITY

Malaria intensity	Agreement (%)	False positive rates (%)[a]	False negative rates (%)[b]
Malaria free	95.9	26.3	4.1
Malaria near water	90.0	5.9	10.0
Moderate malaria	72.3	19.0	27.7
Intense malaria	86.6	19.6	13.4
All categories	83.9	16.1	16.1

a. Omission error; b. commission error.

TABLE 4. TEN MOST DISCRIMINATING RS VARIABLES BY RANK

Rank	Predictor variable	*kappa* statistic
1	Mean Price LST	0.464
2	CCD variance	0.562
3	CCD phase3	0.639
4	DEM	0.691
5	CCD phase2	0.712
6	LST phase1	0.735
7	T_{air} phase1	0.752
8	MIR amp3	0.763
9	NDVI amp2	0.779
10	T_{air} amp3	0.782

LST = Price land surface temperature, CCD = cold cloud duration, T_{air} = air temperature, MIR = mid-infrared, amp2 = amplitude of biannual cycle, amp3 = amplitude of triannual cycle, phase1 = timing of annual cycle, phase2 = timing of biannual cycle, phase3 = timing of triannual cycle.

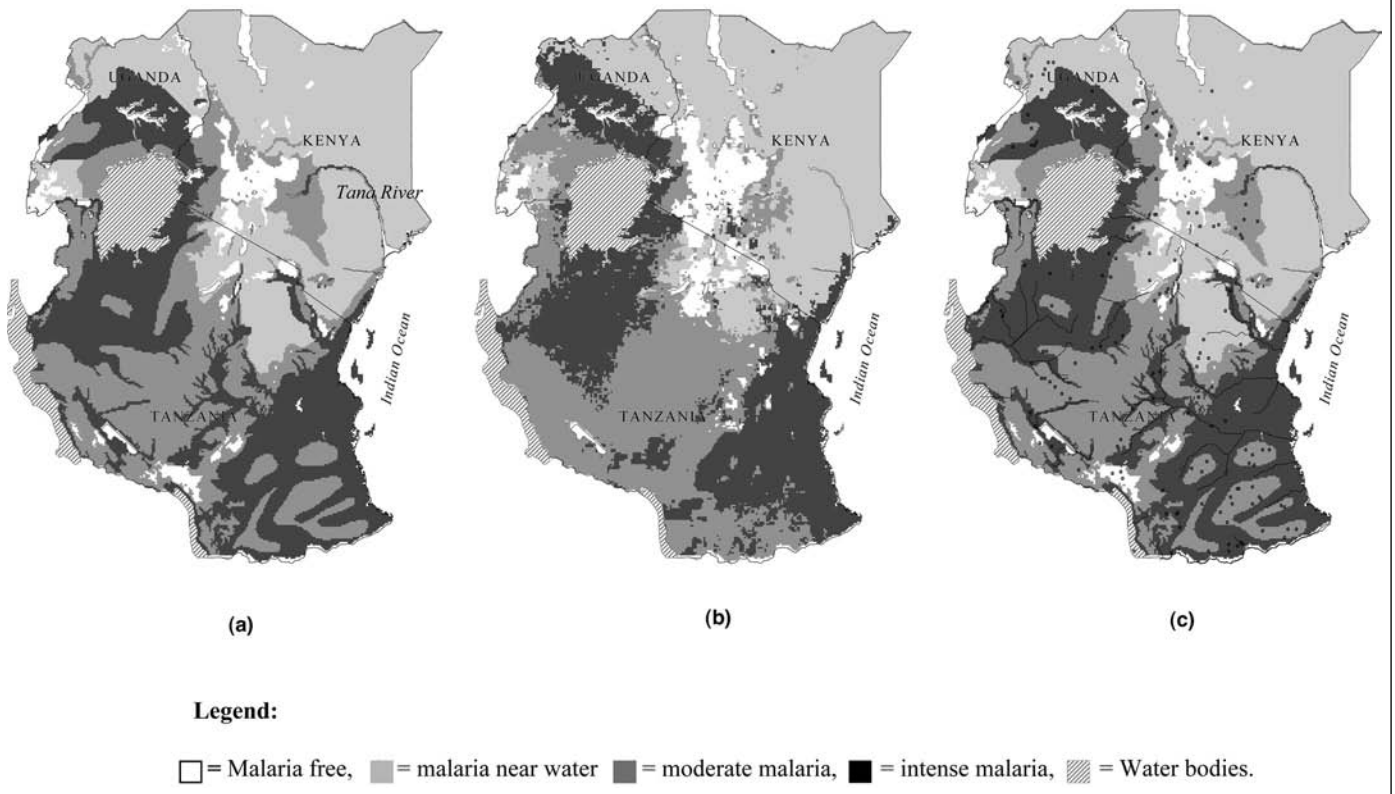

Figure 2. (a) Historical malaria transmission intensity map. (b) Map of discriminant analysis predictions of malaria transmission intensity. (c) Distribution of misclassified pixels (*x*) and main river systems in Tanzania in relation to historical malaria transmission intensity map.

all year round, they usually peak annually, and the DA picks up the timing of the annual cycles of LST and T_{air} in these areas. Furthermore, aside from providing good definitions of areas that do not support stable transmission, stable transmission areas are defined more clearly than models that have used other statistical procedures (Craig *et al.*, 1999).

There is additional scope for the refinement of the climate-based model in several areas; the rationale for this would depend on the level of detail of the information required for use in decision support for malaria control purposes. The inclusion of additional databases such as rivers and other smaller permanent water bodies and the use of higher spatial resolution RS data may improve prediction in the moderate and intense transmission areas in Tanzania and Uganda. Historical maps, however, are likely to be inaccurate at higher resolution and, perhaps, appropriate empirical data could be used to improve the accuracy of predictions. The aim of this study was to demonstrate the utility of RS data in predicting malaria transmission intensity, and the challenge of future research will be to use empirical data to assess the accuracy of these predictions.

Acknowledgments

Information used in this study includes data produced through funding from the Earth Observing System Pathfinder Program of NASA's Mission to Planet Earth in cooperation with National Oceanic and Atmospheric Administration. The data were provided by the Earth Observing Data and Information System (EODIS), Distributed Active Archive Center at Goddard Space Flight Center which archives, manages, and distributes this dataset. Thanks are also due to Fred Snidjers of the Food and Agriculture Organisation's (FAO) Africa Real Time Environmental Monitoring using Imaging Satellites (ARTEMIS) project for permission to use Meteosat CCD data. We also thank Jennifer Small for help in implementing methods developed at the University of Maryland Department of Geography for the derivation of air temperature estimates from AVHRR data. J.A. Omumbo is supported by a Wellcome Trust prize studentship (#060063), S.I. Hay is supported on a Wellcome Trust Advanced Training Fellowship (#056642), and R.W. Snow is on a Wellcome Trust Senior Fellowship (#033340). This paper is published with the permission of the Director, KEMRI.

References

Boyd, D., and P. Curran, 1998. Using remote sensing to reduce uncertainties in the global carbon budget: The potential of radiation acquired in the middle infrared wavelengths, *Remote Sensing Reviews*, 16:293–327.

Boyd, M.F., 1930. *An Introduction to Malariology*, Harvard University Press, Cambridge, Massachusetts, 1438 p.

Brooker, S., S.I. Hay, and D.A.P. Bundy, 2002. Tools from ecology to evaluate infection risk models, *Trends in Parasitology*, in press.

Clarke University, 1997. *IDRISI Version 2.0 for Windows*, Clarke University, Graduate School of Geography, Worcester, Massachusetts, http://www.idrisi.clarku.edu.

Clyde, D.F., 1967. *Malaria in Tanzania*, Oxford University Press, London, New York.

Cohen, J., 1960. A co-efficient of agreement for nominal scale, *Educational and Psychological Measurements*, 20:37–46.

Cracknell, A., 1997. Channel 3: The neglected channel, *The Advanced Very High Resolution Radiometer*, Taylor & Francis, London, pp. 321–342.

Craig, M.H., R.W. Snow, and D. Le Sueur, 1999. A climate-based distribution model of malaria transmission in sub-Saharan Africa, *Parasitology Today*, 15(3):105–111.

Detinova, T.S., 1962. *Age Grouping Methods in Diptera of Medical Importance, with Special Reference to Some Vectors of Malaria*, World Health Organization, Geneva, Switzerland, 210 p.

Dugdale, G., V. McDougall, and V. Thorne, 1995. The TAMSAT method for estimating rainfall over Africa and it's implications, RSS95: *Proceedings of the 21st Annual Conference of the Remote Sensing Society*, 11–14 September, Southampton, England, pp. 773–780.

Dutta, H.M., and A.K. Dutt, 1978. Malaria ecology: a global perspective, *Social Science in Medicine Part D (Medical Geography)*, 12:69–84.

Garrett-Jones, C., 1964. Prognosis for interruption of malaria transmission through assessment of the mosquito's vectorial capacity, *Nature*, 204:1173–1175.

Gesch, D.B., and K.S. Larson, 2000. *Techniques for Development of Global 1-Kilometer Digital Elevation Models*, United States Geological Survey—EROS data centre, Sioux Falls, South Dakota, (http://ededaac.usgs.gov/gtopo30/papers/geschtxt.html).

Gill, C.A., 1920. The role of meteorology in malaria, *Indian Journal of Medical Research*, 8:633–693.

Gilles, H., 1993. Epidemiology of malaria, *Bruce-Chwatt's essential malariology* (E. Arnold, editor), Oxford University Press., Inc., New York, N.Y., pp. 124–163.

Goetz, S., S. Prince, and J. Small, 2000. Advances in satellite remote sensing of environmental variables for epidemiological applications, *Advances in Parasitology*, 47:289–307.

Government of Kenya, 1970. *National Atlas of Kenya*, Survey of Kenya, Nairobi, Kenya, 44 p.

Government of Tanganyika, 1956. *Atlas of Tanganyika, East Africa*, Government Press, Dar es Salaam, Tanganyika, 29 p.

Government of Uganda, 1962. *Atlas of Uganda*, Department of Lands and Surveys, Kampala, Uganda, 83 p.

Hay, S.I., and J.J. Lennon, 1999. Deriving meteorological variables across Africa for the study and control of vector-borne disease: A comparison of remote sensing and spatial interpolation of climate, *Tropical Medicine & International Health*, 4(1):58–71.

Hay, S.I., J.A. Omumbo, M.H. Craig, and R.W. Snow, 2000a. Earth observation, geographic information systems and *Plasmodium falciparum* malaria in sub-Saharan Africa, *Advances in Parasitology*, 47:173–215.

Hay, S.I., M.J. Packer, and D.J. Rogers, 1997. The impact of remote sensing on the study and control of invertebrate intermediate hosts and vectors for disease, *International Journal of Remote Sensing*, 18(14):2899–2930.

Hay, S.I., D.J. Rogers, J.F. Toomer, and R.W. Snow, 2000b. Annual *Plasmodium falciparum* entomological inoculation rates (EIR) across Africa: Literature survey, internet access and review, *Transactions of the Royal Society of Tropical Medicine and Hygiene*, 94:113–127.

Hay, S.I., R.W. Snow, and D.J. Rogers, 1998. Predicting malaria seasons in Kenya using multi-temporal meteorological satellite sensor data, *Transactions of the Royal Society of Tropical Medicine and Hygiene*, 92:12–20.

Hay, S.I., C.J. Tucker, D.J. Rogers, and M.J. Packer, 1996. Remotely sensed surrogates of meteorological data for the study of the distribution and abundance of arthropod vectors of disease, *Annals of Tropical Medicine and Parasitology*, 90:1–19.

James, M.E., and S.N.V. Kalluri, 1994. The Pathfinder AVHRR land data set—an improved coarse resolution data set for terrestrial monitoring, *International Journal of Remote Sensing*, 15: 3347–3363.

Kleinschmidt, I., M. Bagayoko, G.P.Y. Clarke, M.H. Craig, and D. Le Sueur, 2000. A spatial statistical approach to malaria mapping, *International Journal of Epidemiology*, 29(2):355–361.

Landis, J., and G. Koch, 1977. The measurement of observer agreement for categorical data, *Biometrics*, 33:159–174.

Lindsay, S.W., and M.H. Birley, 1996. Climate change and malaria transmission, *Annals of Tropical Medicine and Parasitology*, 90(6):573–588.

Lysenko, A.Y., and A.E. Beljaev, 1969. An analysis of the distribution of *Plasmodium ovale, Bulletin of the World Health Organization*, 40:383–394.

Macdonald, G., 1957. *The Epidemiology and Control of Malaria*, Oxford University Press, London, 310 p.

MapInfo Corporation, 1985–2000. *MapInfo Professional*, MapInfo Corporation, Troy, New York (software).

MARA/ARMA collaboration, 1998. *Towards an Atlas of Malaria Transmission in Africa: First Technical Report of the MARA/ARMA*, South African Medical Research Council, IDRC, Canada and Wellcome Trust, UK, Durban, South Africa, 30 p.

Myneni, R.B., S. Maggion, J. Iaquinta, J.L. Privette, N. Gobron, B. Pinty, D.S. Kimes, M.M. Verstraete, and D.L. Williams, 1995. Optical remote sensing of vegetation: Modeling, caveats and algorithms, *Remote Sensing of Environment*, 51:169–188.

Nicholson, S.E., M.L. Davenport, and A.R. Malo, 1990. A comparison of vegetation response to rainfall in the Sahel and East Africa using Normalized Difference Vegetation Index from NOAA-AVHRR, *Climate Change*, 17:209–241.

Onori, E., 1967. Distribution of *Plasmodium ovale* in the Eastern, Western and Northern regions of Uganda, *Bulletin of the World Health Organization*, 37(4):665–668.

Patz, J.A., K. Strzepek, S. Lele, M. Hedden, S. Greene, B. Noden, S.I. Hay, L. Kalkstein, and J.C. Beier, 1998. Predicting key malaria transmission factors, biting and entomological inoculation rates, using modelled soil moisture in Kenya, *Tropical Medicine & International Health*, 3(10):818–827.

Price, J., 1984. Land surface temperature measurements from the split window channels of the NOAA Advanced Very High Resolution Radiometer, *Journal of Geophysical Research*, 89:7231–7237.

Rogers, D.J., 2000. Satellites, space, time and the African trypanosomiases, *Advances in Parasitology*, 47:129–171.

Rogers, D.J., S.I. Hay, and M.J. Packer, 1996. Predicting the distribution of tsetse-flies in West Africa using temporal Fourier processed meteorological satellite data, *Annals of Tropical Medicine and Parasitology*, 90:225–241.

Rogers, D.J., S.E. Randolph, R.W. Snow, and S.I. Hay, 2002. Satellite imagery in the study and forecast of malaria, *Nature*, in press.

Snow, R.W., M.H. Craig, U. Deichmann, and K. Marsh, 1999. Estimating mortality an disability due to malaria among Africa's non-pregnant population, *Bulletin of the World Health Organization*, 77(8):624–640.

Snow, R.W., E. Gouws, J. Omumbo, B. Rapuoda, M.H. Craig, F.C. Tanser, D. le Sueur, and J. Ouma, 1998. Models to predict the intensity of Plasmodium falciparum transmission: applications to the burden of disease in Kenya, *Transactions of the Royal Society of Tropical Medicine and Hygiene*, 92(6):601–606.

Snow, R.W., K. Marsh, and D. Le Sueur, 1996. The need for maps of transmission intensity to guide malaria control in Africa, *Parasitology Today*, 12:455–456.

Tanser, F.C., 2000. *The Application of Geographical Information Systems to Infectious Diseases and Health Systems in Africa*, Faculty of Medicine, University of Natal, Durban, South Africa, 168 p.

Thomson, M.C., S.J. Connor, U. D'Alessandro, B. Rowlinson, P. Diggle, M. Cresswell, and B.M. Greenwood, 1999. Predicting malaria infection in Gambian children from satellite data and bed net use surveys: The importance of spatial correlation in the interpretation of results, *American Journal of Tropical Medicine and Hygiene*, 61(1):2–8.

Tucker, C.J., 1979. Red and photographic infrared linear combinations for monitoring vegetation, *Remote Sensing of Environment*, 8:127–150.

Tucker, C.J., and P. Sellers, 1986. Satellite remote sensing of primary production, *International Journal of Remote Sensing*, 7: 1395–1416.

WHO, 1999. *The World Health Report 1999: Making a Difference*, World Health Organization, Geneva, Switzerland, 122 p.